Inorg. Chem. **2007**, *46*, 4079–4089

Remarkable Steric Effects and Influence of Monodentate Axial Ligands L on the Spin-Crossover Properties of *trans*-[$Fe^{II}(N_4$ ligand)L] Complexes

José Sánchez Costa,[†] Kristian Lappalainen,[†] Graham de Ruiter,[†] Manuel Quesada,[†] Jinkui Tang,[†] Ilpo Mutikainen,[‡] Urho Turpeinen,[‡] C. Matthias Grunert,[§] Philipp Gütlich,[§] Hanane Zhor Lazar,[||] Jean-François Létard,[||] Patrick Gamez,[†] and Jan Reedijk*,[†]

Leiden Institute of Chemistry, Leiden University, P.O. Box 9502, 2300 RA Leiden, The Netherlands, Department of Chemistry, Laboratory of Inorganic Chemistry, University of Helsinki, P.O. Box 55, A. I. Virtasenaukio 1, 00014, Helsinki, Finland, Institut für Anorganische und Analytische Chemie, Johannes-Gutenberg-Universität, Staudinger-Weg 9, D-55099 Mainz, Germany, and Groupe des Sciences Moléculaires, Institut de Chimie de la Matière Condensée de Bordeaux, UPR CNRS No. 9048, Université Bordeaux I, 87 Av. Doc. A. Schweitzer, F-33608 Pessac, France

Received December 15, 2006

Iron(II) complexes obtained from tetradentate, rigid, linear N_4 ligands have been investigated to appraise the influence of steric effects and the impact of trans-coordinated anions on the spin-transition behavior. As expected, the well-designed ligands embrace the metal center, resulting in octahedral iron(II) complexes where the basal plane is fully occupied by the pyridine/pyrazole N_4 ligand, while anions or solvent molecules are exclusively axially coordinated. Precursor complexes, namely, $[Fe(bpzbpy)(MeOH)_2](BF_4)_2$ (where bpzbpy symbolizes the ligand 6,6′-bis(*N*-pyrazolylmethyl)-2,2′-bipyridine) and $[Fe(mbpzbpy)(MeOH)_2](BF_4)_2$ (where mbpzbpy symbolizes the ligand 6,6′-bis-(3,5-dimethyl-*N*-pyrazolmethyl)-2,2′-bipyridine), have been used for the in situ preparation of a series of structural analogues via the exchange of the weakly coordinated trans methanol molecules by various anions, such as thiocyanate, selenocyanate, or dicyanamide. The magnetic properties of all seven iron(II) compounds thus obtained have been investigated. Two iron(II) complexes, i.e., $[Fe(bpzbpy)(NCS)_2]$ and $[Fe(bpzbpy)(NCSe)_2]$, exhibit gradual spin-crossover (SCO) properties typical of isolated mononuclear species with weak cooperative interaction. These two SCO materials have been studied by Mössbauer spectroscopy, and the light-induced excited spin state trapping effect has been investigated, revealing the possibility to induce the spin-transition both by temperature variation and by light irradiation. A correlation between steric/anion effect and SCO behavior is suggested.

Introduction

The phenomenon of spin-crossover in iron(II) coordination compounds has been first reported by König and Madeja 40 years ago.[1] Since then, a continuous scientific interest for its comprehension,[2−5] as well as for the design and preparation of such complexes, has been observed,[6,7] driven by the potential applications as molecular switches, data storage materials, and data displays.[8,9] Thus, a number of pseudo-octahedral FeN_6 complexes[10] have been described to undergo transitions between high-spin (HS, $S = 2$, $^5T_2$) and low-spin (LS, $S = 0$, $^1A_1$) states under the influence of an external

* To whom correspondence should be addressed. E-mail: reedijk@chem.leidenuniv.nl. Phone: +31715274459. Fax: +31715274671.
[†] Leiden Institute of Chemistry.
[‡] University of Helsinki.
[§] Johannes-Gutenberg-Universität.
[||] Université Bordeaux I.

(1) König, E.; Madeja, K. *Chem. Commun.* **1966**, 61−62.
(2) Kahn, O.; Codjovi, E. *Philos. Trans. R. Soc. London, Ser. A* **1996**, *354*, 359−379.
(3) Bousseksou, A.; Molnar, G.; Matouzenko, G. *Eur. J. Inorg. Chem.* **2004**, 4353−4369.
(4) Kahn, O. *Molecular Magnetism*; VCH: New York, 1993.
(5) Gütlich, P.; Hauser, A.; Spiering, H. *Angew. Chem., Int. Ed. Engl.* **1994**, *33*, 2024−2054.
(6) Zhuang, Z. J.; Tao, J. Q.; Yu, Z.; Dun, C. Y.; Liu, Y. J.; You, X. Z. *J. Chem. Soc., Dalton Trans.* **1998**, 327−328.
(7) Gütlich, P.; Garcia, Y.; Goodwin, H. A. *Chem. Soc. Rev.* **2000**, *29*, 419−427.
(8) Kahn, O.; Martinez, C. J. *Science* **1998**, *279*, 44−48.
(9) Létard, J. F.; Guionneau, P.; Goux-Capes, L. *Top. Curr. Chem.* **2004**, *235*, 221−249.
(10) Moliner, N.; Munoz, M. C.; Létard, S.; Salmon, L.; Tuchagues, J. P.; Bousseksou, A.; Real, J. A. *Inorg. Chem.* **2002**, *41*, 6997−7005.

10.1021/ic0624017 CCC: $37.00
Published on Web 04/19/2007

stimulus, i.e., temperature, pressure, or light.[11] The resulting main structural changes affect the geometry of the FeN_6 core, since the Fe−N bond lengths decrease when the iron(II) centers go from paramagnetic HS to diamagnetic LS state[12] and the N−Fe−N angles experience strong variations toward a regular octahedral geometry.[1,13−15]

It has been observed that minor intramolecular structural features within the coordination sphere of mononuclear iron(II) compounds could lead to drastic modifications of the magnetic properties.[16] A well-known example of such structural impact on the physical properties relates to $[Fe(bpy)_2(NCS)_2]$ which crystallizes as three different polymorphs (known as polymorphs I, II, and III), all exhibiting different magnetic behaviors.[16,17] Polymorph II has been characterized as *cis*-$[Fe(bpy)_2(NCS)_2]$, with two isocyanates at equatorial positions of the octahedron.[16] It has been proposed that one of the two other polymorphs may actually be the trans isomer of the previous compound, thus having isocyanate anions coordinated at the axial positions.[18] Such cis/trans variation in the coordination geometry of complexes with bidentate ligands is likely to occur, and indeed an intriguing example has been recently reported.[19] Reaction of iron(II) chloride with 2-picolylamine (pic) leads to the expected octahedral $[Fe(pic)_2Cl_2]$ complex, but both the cis and the trans isomers are formed, which cocrystallize in a 1:1 ratio.[19] One simple approach to decrease the number of accessible coordination isomers is then to increase the number of donor atoms via the design and preparation of multidentate ligands. In the present study, the preparation of iron(II) compounds with new tetradentate ligands is reported. However, it has to be mentioned that cis/trans isomerism is still possible with linear tetradentate ligands, depending on their flexibility. For instance, N_4 flexible ligands will give rise to the cis-α and cis-β geometries (Figure S1a,b in Supporting Information), while rigid ones will only lead to trans complexes (Figure S1c).[20] For that reason, we have decided to synthesize rigid bipyridine-based ligands of the type depicted in Chart 1. This synthetic strategy is driven by the fact that bipyridine,[17,21] pyrazole,[22,23] or pyridine−pyrazole[24,25] derivatives are prime ligands to obtain iron(II) spin-crossover coordination compounds. The second objective is to generate octahedral iron(II) complexes whose equatorial plane of the metal coordination sphere is fully occupied by the embracing N_4 ligand. Such control of the coordination geometry is thus expected to allow a fine-tuning of the ligand-field strength determined by the nature of the axial ligands used. This geometric constraint is more difficult (or even impossible) to achieve with bidentate ligands, and for example, reaction of $FeCl_2$ with bis(1-pyrazolyl)methane (bpm) produces *cis*-$[Fe(bpm)_2Cl_2]$, while *trans*-$[Fe(bpm)_2(NCS)_2]$ is obtained when the $Fe(NCS)_2$ salt is used.[22]

Chart 1. [Bipyridine-bis(pyrazole)]-Based Ligands

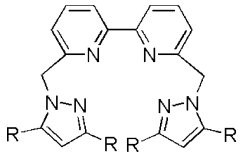

R = H, CH_3

In this Article, the preparation and full characterization of iron(II) complexes obtained from two new N_4 ligands, namely, 6,6′-bis(*N*-pyrazolylmethyl)-2,2′-bipyridine (bpzbpy, Chart 1, R = H) and 6,6′-bis(3,5-dimethyl-*N*-pyrazolmethyl)-2,2′-bipyridine (mbpzbpy, Chart 1, R = CH_3), are described. The different mononuclear coordination compounds obtained exhibit distinct magnetic behaviors rising from the different axial ligands.

Experimental Section

General Remarks. All chemicals were of reagent grade and were used as commercially obtained. Elemental analyses for C, H, and N were performed with a Perkin-Elmer 2400 analyzer. FTIR spectra were recorded with a Perkin-Elmer Paragon 1000 FTIR spectrophotometer equipped with a Golden Gate ATR device, and the reflectance technique (4000−300 cm^{-1}) was used. ^1H NMR and ^{13}C NMR spectra were recorded on a Bruker DPX 300 (300 MHz) instrument. Chemical shifts are reported in δ (parts per million) relative to an internal standard of tetramethylsilane. ESI mass analyses were carried out on a Voyager Elite from PerSeptive Biosystems.

Iron(II) triflate was synthesized in warm water, from iron(0) powder (Acros) and triflic acid (Aldrich). After filtration of the remaining metal (slight excess), water was evaporated under reduced pressure, yielding a white solid formulated as $Fe(CF_3SO_3)_2 \cdot 2H_2O$ by elemental analysis.

Synthesis of the Ligands. The ligands 6,6′-bis(*N*-pyrazolylmethyl)-2,2′-bipyridine (bpzbpy) and 6,6′-bis(3,5-dimethyl-*N*-pyrazolmethyl)-2,2′-bipyridine (mbpzbpy) were prepared from 6,6′-bis(bromomethyl)-2,2′-bipyridine.[26]

Bpzbpy. A solution of 0.44 g of pyrazole (6.5 mmol) in dry THF (30 mL) was added dropwise to a suspension of NaH (0.15 g, 6.5 mmol) in 30 mL of dry THF. The resulting reaction mixture was refluxed for 2 h, and a solution of 6,6′-bis(bromomethyl)-2,2′-

(11) Gütlich, P.; Goodwin, H. A. *Top. Curr. Chem.* **2004**, *233*, 1−47.
(12) Niel, V.; Gaspar, A. B.; Muñoz, M. C.; Abarca, B.; Ballesteros, R.; Real, J. A. *Inorg. Chem.* **2003**, *42*, 4782−4788.
(13) Alvarez, S. *J. Am. Chem. Soc.* **2003**, *125*, 6795−6802.
(14) Matouzenko, G. S.; Luneau, D.; Molnar, G.; Ould-Moussa, N.; Zein, S.; Borshch, S. A.; Bousseksou, A.; Averseng, F. *Eur. J. Inorg. Chem.* **2006**, 2671−2682.
(15) Hauser, A. *Top. Curr. Chem.* **2004**, *233*, 49−58.
(16) Konno, M.; Mikami-Kido, M. *Bull. Chem. Soc. Jpn.* **1991**, *64*, 339−345.
(17) König, E.; Madeja, K.; Watson, K. J. *J. Am. Chem. Soc.* **1968**, *90*, 1146−1153.
(18) Guionneau, P.; Marchivie, M.; Bravic, G.; Létard, J. F.; Chasseau, D. *Top. Curr. Chem.* **2004**, *234*, 97−128.
(19) Tornroos, K. W.; Chernyshov, D.; Hostettler, M.; Bürgi, H. B. *Acta Crystallogr. C* **2005**, *61*, M450−M452.
(20) Britovsek, G. J. P.; England, J.; White, A. J. P. *Dalton Trans.* **2006**, 1399−1408.
(21) Real, J. A.; Gaspar, A. B.; Muñoz, M. C. *Dalton Trans.* **2005**, 2062−2079.
(22) Field, L. D.; Messerle, B. A.; Soler, L. P.; Hambley, T. W.; Turner, P. *J. Organomet. Chem.* **2002**, *655*, 146−157.
(23) Reger, D. L.; Little, C. A.; Young, V. G.; Maren, P. *Inorg. Chem.* **2001**, *40*, 2870−2874.
(24) Carbonera, C.; Costa, J. S.; Money, V. A.; Elhaik, J.; Howard, J. A. K.; Halcrow, M. A.; Létard, J. F. *Dalton Trans.* **2006**, 3058−3066.
(25) Bhattacharjee, A.; Ksenofontov, V.; Sugiyarto, K. H.; Goodwin, H. A.; Gütlich, P. *Adv. Funct. Mater.* **2003**, *13*, 877−882.
(26) Rodriguezubis, J. C.; Alpha, B.; Plancherel, D.; Lehn, J. M. *Helv. Chim. Acta* **1984**, *67*, 2264−2269.

Table 1. Crystal Data and Structure Refinement for [Fe(mbpzbpy)(MeOH)$_2$](BF$_4$)$_2$ (**1**), [Fe(mbpzbpy)(CF$_3$SO$_3$)$_2$] (**2**), [Fe(bpzbpy)(CF$_3$SO$_3$)$_2$] (**3**), [Fe(mbpzbpy)(NCS)$_2$](CH$_3$OH)$_{0.5}$ (**4**), [Fe(bpzbpy)(NCS)$_2$] (**5**), and [Fe(mbpzbpy)(N(CN)$_2$)$_2$] (**7**)

	1	**2**	**3**	**4**	**5**	**7**
formula	$C_{24}H_{32}B_2F_8FeN_6O_2$	$C_{24}H_{24}F_6FeN_6O_6S_2$	$C_{20}H_{16}F_6FeN_6O_6S_2$	$C_{24}H_{24}FeN_8S_2$, 0.5(CH_4O)	$C_{20}H_{16}FeN_8S_2$	$C_{26}H_{24}FeN_{12}$
fw (g mol^{-1})	666.03	726.46	670.36	560.50	488.38	560.42
cryst size (mm^3)	0.30 × 0.30 × 0.22	0.40 × 0.20 × 0.20	0.30 × 0.20 × 0.10	0.22 × 0.13 × 0.02	0.08 × 0.04 × 0.02	0.30 × 0.30 × 0.01
cryst color	yellow	orange	yellow	red	red	red
temperature (K)	173(2)	173(2)	173(2)	173(2)	173(2)	173(2)
cryst syst, space group	triclinic, $P\bar{1}$	triclinic, $P\bar{1}$	monoclinic, $P2_1/n$	triclinic, $P\bar{1}$	monoclinic, $P2_1/n$	monoclinic, $C2/c$
a (Å)	8.936(2)	9.574(2)	12.495(2)	8.112(2)	14.477(3)	20.522(4)
b (Å)	11.823(2)	10.757(2)	14.370(3)	10.671(2)	10.635(2)	14.136(3)
c (Å)	14.563(2)	14.712(2)	13.809(2)	16.026(3)	15.577(3)	9.213(2)
α (deg)	73.17(2)	105.89(3)	90.00	106.21(3)	90.00	90.00
β (deg)	79.54(2)	95.66(3)	92.58(2)	95.15(3)	118.13(3)	106.87(3)
γ (deg)	86.84(2)	90.45(3)	90.00	96.88(3)	90.00	90.00
volume (Å^3)	1448.2(5)	1449.2(5)	2476.9(7)	1311.4(4)	2115.0(7)	2557.7(9)
Z	2	2	4	2	4	4
calcd density (g cm^{-3})	1.527	1.665	1.798	1.419	1.534	1.455
F(000)	684	740	1352	582	1000	1160
abs coeff (mm^{-1})	0.607	0.754	0.875	0.766	0.936	0.632
θ for data collection (deg)	2.84−27.50	2.71−27.50	2.58−27.54	2.67−27.50	2.42−27.86	3.14−27.53
rflns collected (R_{int})	21015 (0.0347)	22613 (0.0456)	39047 (0.0394)	21681 (0.0661)	29317 (0.1124)	20716 (0.0421
data/params	6620/447	6639/406	5683/370	5984/336	4845/314	2936/177
goodness of fit on F^2	1.025	1.016	1.011	1.026	1.025	0.742
R1 (wR2) [$I > 2\sigma(I)$]	0.0460 (0.1180)	0.0388 (0.0968)	0.0723 (0.1860)	0.0398 (0.1070)	0.0668 (0.1609)	0.0350 (0.0920)
largest difference peak and hole (e Å^3)	1.158 and −0.477	0.586 and −0.548	4.397 and −0.874	0.329 and −0.593	0.734 and −0.665	0.589 and −0.541

bipyridine (1.00 g, 2.92 mmol) in 70 mL of dry THF was subsequently added dropwise. The reaction mixture was stirred at room temperature for 24 h. Afterward, the reaction was quenched through the addition of 50 mL of distilled water. THF was evaporated under reduced pressure, and the remaining aqueous phase was extracted with dichloromethane (3 × 50 mL). The pooled organic phase was dried over Na_2SO_4 and filtered, and the solvent was evaporated under reduced pressure. The product bpzbpy was obtained as a white microcrystalline powder. (Yield = 0.75 g, 77%.) ^{1}H NMR ($CDCl_3$, 300 MHz) δ 5.54 (s, 4H, CH_2-py), 6.34 (t, J = 2.1 Hz, 2H, CH-pz), 6.97 (d, J = 7.8 Hz, 2H, H−C(5,5′)), 7.58 (d, J = 2.3 Hz, 2H, CH-pz), 7.59 (d, J = 1.9 Hz, 2H, CH-pz), 7.75 (t, J = 7.8 Hz, 2H, H−C(4,4′)), 8.3 (d, J = 7.9 Hz, 2H, H−C(3,3′)) ppm. ^{13}C NMR ($CDCl_3$, 300 MHz) δ 57.5, 106.2, 120.0, 121.5, 129.9, 137.8, 139.8, 155.4, and 156.1 ppm. MS (m/z) 317 (M^+, 100). IR ν 1575, 1394, 1094, 1083, 1052, 780, 764, 626 cm^{-1}.

Mbpzbpy. This ligand was prepared following the same experimental procedure (see above), using 0.09 g (3.74 mmol) of NaH, 0.360 g (3.74 mmol) of 3,5-dimethylpyrazole, and 0.58 g (1.68 mmol) of 6,6′-bis(bromomethyl)-2,2′-bipyridine. The product was obtained as a white powder. (Yield = 0.66 g, 94%.) ^{1}H NMR ($CDCl_3$, 300 MHz) δ 2.24 and 2.26 (s, 6H, CH_3-pz), 5.40 (s, 4H, CH_2-py), 5.89 (s, 2H, CH-pz), 6.83 (d, J = 7.6 Hz, 2H, H−C(5,5′)), 7.72 (t, J = 7.8 Hz, 2H, H−C(4,4′)), 8.27 (d, J = 7.7 Hz, 2H, H−C(3,3′)) ppm. ^{13}C NMR ($CDCl_3$, 300 MHz) δ 11.2, 13.5, 54.5, 105.7, 119.7, 121.0, 137.9, 139.8, 148.0, 155.4, and 156.8 ppm. MS (m/z) 372 (M^+, 100). IR ν 1572, 1550, 1425, 785, 780, 602 cm^{-1}.

Preparation of the Complexes. Coordination compounds **1**−**3** were prepared as follows: A solution of the corresponding iron(II) salt (0.134 mmol) in 10 mL of methanol was added to a solution of the ligand (0.134 mmol) in 10 mL of methanol. The resulting reaction mixture was stirred for 10 min and subsequently filtered. The filtrate was left unperturbed for the slow evaporation of the solvent.

[Fe(mbpzbpy)(MeOH)$_2$](BF$_4$)$_2$ (1). Yellow block crystals, suitable for X-ray structure determination, were obtained after 2 days. (Yield = 67.8 mg, 76%.) Anal. Calcd for $C_{24}H_{32}B_2F_8FeN_6O_2$: C, 43.3; H, 4.8; N, 12.6. Found: C, 42.9; H, 4.8; N, 12.7.

[Fe(mbpzbpy)(CF$_3$SO$_3$)$_2$] (2). Orange block crystals, suitable for X-ray structure determination, were obtained after 2 days. (Yield = 78.8 mg, 81%.) Anal. Calcd for $C_{24}H_{24}F_6FeN_6O_6S_2$: C, 39.7; H, 3.3; N, 11.6. Found: C, 39.6; H, 3.3; N, 11.6.

[Fe(bpzbpy)(CF$_3$SO$_3$)$_2$] (3). Yellow prismatic crystals, suitable for X-ray structure determination, were obtained after 3 days. (Yield = 74.6 mg, 83%.) Anal. Calcd for $C_{20}H_{16}F_6FeN_6O_6S_2$: C, 35.8; H, 2.4; N, 12.5. Found: C, 35.4; H, 2.5; N, 12.3.

Complexes **4**−**7** were synthesized according to the following procedure: A solution of iron(II) tetrafluoroborate hexahydrate (45.2 mg, 0.134 mmol) in 10 mL of methanol was added to a solution of the corresponding ligand (0.134 mmol) in 10 mL of methanol. After 10 min of stirring, 26.8 mmol of the sodium salt of different counterions (namely, thiocyanate, selenocyanate, or dicyanamide) was added to the reaction mixture. The solution was further stirred for 10 min and filtered. The filtrate was left unperturbed for the slow evaporation of the solvent.

[Fe(mbpzbpy)(NCS)$_2$](CH$_3$OH)$_{0.5}$ (4). Red plate crystals, suitable for X-ray structure determination, were obtained after 1 day. (Yield = 60.1 mg, 80%.) Anal. Calcd for $C_{24}H_{24}FeN_8S_2$ (**4**·0.5 MeOH): C, 52.9; H, 4.4; N, 20.6. Found: C, 53.0; H, 4.5; N, 20.3.

[Fe(bpzbpy)(NCS)$_2$] (5). Red needle crystals, suitable for X-ray structure determination, were obtained after 1 day. (Yield = 55.6 mg, 85%.) Anal. Calcd for $C_{20}H_{16}FeN_8S_2$ (**5**): C, 49.2; H, 3.3; N, 22.9. Found: C, 49.1; H, 3.3; N, 22.8.

[Fe(bpzbpy)(NCSe)$_2$] (6). A microcrystalline powder was obtained after 1 day. (Yield = 70.2 mg, 90%.) Anal. Calcd for $C_{20}H_{16}FeN_8Se_2$: C, 41.3; H, 2.8; N, 19.3. Found: C, 41.3; H, 3.0; N, 19.4.

[Fe(mbpzbpy)(N(CN)$_2$)$_2$] (7). Red plate crystals, suitable for X-ray structure determination, were obtained after 2 days. (Yield = 56.3 mg, 75%.) Anal. Calcd for $C_{26}H_{24}FeN_{12}$: C, 55.7; H, 4.3; N, 30.0. Found: C, 55.4; H, 4.4; N, 30.2.

Magnetic Measurements. Magnetic susceptibility measurements were carried out using a Quantum Design MPMS-5 5T SQUID magnetometer at 5000 Oe in the temperature range 5−300 K. Data were corrected for the diamagnetic contributions estimated from Pascal's tables.[4]

Mössbauer Spectroscopy. ^{57}Fe Mössbauer spectra were recorded using a constant-acceleration conventional spectrometer and helium

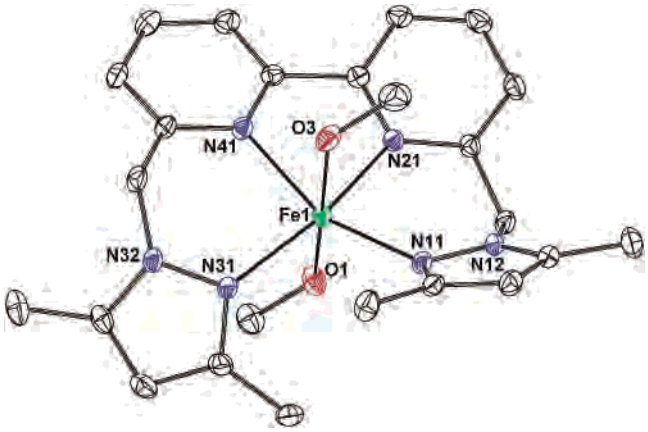

Figure 1. ORTEP view of the cation of $[Fe(mbpzbpy)(MeOH)_2](BF_4)_2$ (**1**) at the 30% probability level. Hydrogen atoms are omitted for clarity.

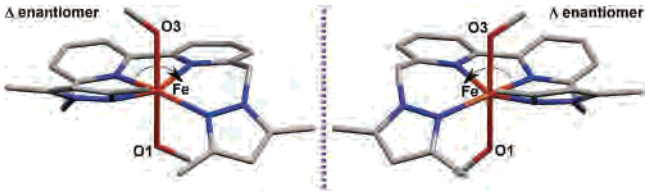

Figure 2. Enantiomorphs of $[Fe(bpzbpy)(MeOH)_2](BF_4)_2$ (**1**) which cocrystallize in a 1:1 ratio.

bath cryostat or nitrogen cryostat. The sample and the Mössbauer source ^{57}Co/Rh were immersed in liquid helium to record the spectra at 4.2 K. The Recoil 1.03a Mössbauer analysis software was used to fit the experimental spectra.[27]

Photomagnetism. The reflectivity of the different complexes was investigated using a custom-built reflectivity setup equipped with a CVI spectrometer. Reflectivity spectra within the range 450−950 nm at a given temperature and the temperature dependence of the signal at a selected wavelength (±2.5 nm) between 5 and 290 K were simultaneously recorded. The light source is a halogen lamp emitting between 400 and 900 nm. These analyses were directly performed at the surface of thin layers of powder samples without any dispersion in a matrix.

The photomagnetic measurements were performed using a Spectra Physics Series 2025 Kr^+ laser (λ = 532 nm) coupled through an optical fiber to the cavity of a Quantum Design MPMS-55 SQUID magnetometer operating at 2−300 K with an external magnetic field of 2 T.[28] The power of the laser beam on the sample was adjusted to 5 mW cm^{-2}. Calibrations have been performed to determine the exact intensity of light received by the sample. Furthermore, it has been experimentally verified that no jump in the magnetic response is occurring upon switching off the laser beam. Such an artificial effect was, in fact, evidence that a heating effect is happening on the sample.[28] Bulk attenuation of light intensity was limited using a thin layer of the sample to be analyzed. It is noteworthy that there was no change in the data due to sample heating upon laser irradiation. The mass of these thin-layer samples, approximately 0.2 mg, was graphically estimated by comparison of the current thermal spin-crossover plot with the one obtained for an accurately weighed sample of the same compound. The data were corrected for the magnetization of the sample holder and for diamagnetic contributions, estimated from Pascal's constants.[4]

(27) Rancourt, D. G.; Lagarec, K. *Nucl. Instrum. Methods Phys. Res.* **1997**, *B129*, 266.
(28) Létard, J. F. *J. Mater. Chem.* **2006**, *16*, 2550−2559.

Table 2. Selected Bond Lengths (Å) and Angles (deg) in $[Fe(mbpzbpy)(MeOH)_2](BF_4)_2$ (**1**)

Bond Distance			
Fe1−N31	2.137(2)	Fe1−N11	2.146(2)
Fe1−N21	2.183(2)	Fe1−N41	2.186(2)
Fe1−O1	2.192(2)	Fe1−O3	2.198(2)
Bond Angle			
N11−Fe1−N21	90.08(8)	N21−Fe1−N41	75.88(8)
N41−Fe1−N31	90.52(8)	N31−Fe1−N11	107.07(8)
O1−Fe1−O3	172.60(7)		

X-ray Crystallographic Analysis and Data Collection. Crystallographic data and refinement details are given in Table 1. A crystal was selected for the X-ray measurements and mounted to the glass fiber using the oil drop method,[29] and data were collected at 173 K on a Nonius Kappa CCD diffractometer (Mo Kα radiation, graphite monochromator, λ = 0.710 73). The intensity data were corrected for Lorentz and polarization effects and for absorption. The programs COLLECT,[30] SHELXS-97,[31] and SHELXL-97[32] were used for data reduction, structure solution, and structure refinement, respectively. The non-hydrogen atoms were refined anisotropically. The H atoms were introduced in calculated positions and refined with fixed geometry with respect to their carrier atoms.

Results and Discussion

Description of Structures. Stereochemistry. All the octahedral $[Fe(N_4\ ligand)L_2]$ (N_4 ligand = mbpzbpy or bpzbpy, L = anion or solvent molecule) complexes prepared exclusively possess the expected stereochemistry. Indeed, as anticipated, the rigid linear N_4 ligand is coordinated at the four equatorial positions of the octahedron. Its lack of flexibility prevents the formation of the cis-α and the cis-β isomers (Figure S1). As a result, the axial positions are occupied by anions or solvent molecules, which are trans to each other. No relevant $\pi-\pi$ interactions between coordinated ligands of neighboring $[Fe(N_4\ ligand)]^{2+}$ cations and/or intermolecular contacts are observed in the crystal packing of all coordination compounds reported in the present study. This lack of cooperativity between the iron(II) centers corroborates the magnetic behaviors of complexes **5** and **6**.

Crystal Structure of $[Fe(mbpzbpy)(MeOH)_2](BF_4)_2$ (1). Compound **1** crystallizes in the $P\bar{1}$ triclinic space group. An ORTEP perspective view of the cationic moiety of **1** is shown in Figure 1. Selected bond lengths and angles are given in Table 2. The unit cell contains two iron compounds **1** (Z = 2) which are enantiomeric isomers (Figure 2). The $[FeN_4O_2]$ octahedron is strongly distorted, most likely due to the small bite angle of the bipyridine moiety. Thus, the Fe−N distances involving the bipyridine unit are longer (Fe−N21 = 2.183(2) Å, Fe−N41 = 2.186(2) Å) than the pyrazole ones (Fe−N11 = 2.146(2) Å, Fe−N31 = 2.137(2) Å). However, these Fe−N bond lengths are typical for high-spin iron(II) centers.[33] The axial positions are occupied by methanol

(29) Kottke, T.; Stalke, D. *J. Appl. Crystallogr.* **1993**, *26*, 615−619.
(30) *COLLECT*; Nonius BV: Delft, The Netherlands, 2002.
(31) Sheldrick, G. M. *SHELXS-97 Program for Crystal Structure Determination*; University of Göttingen: Göttingen, Germany, 1997.
(32) Sheldrick, G. M. *SHELXL-97-2 Program for Crystal Structure Refinement*; University of Göttingen: Göttingen, Germany, 1997.
(33) Leita, B. A.; Moubaraki, B.; Murray, K. S.; Smith, J. P. *Polyhedron* **2005**, *24*, 2165−2172.

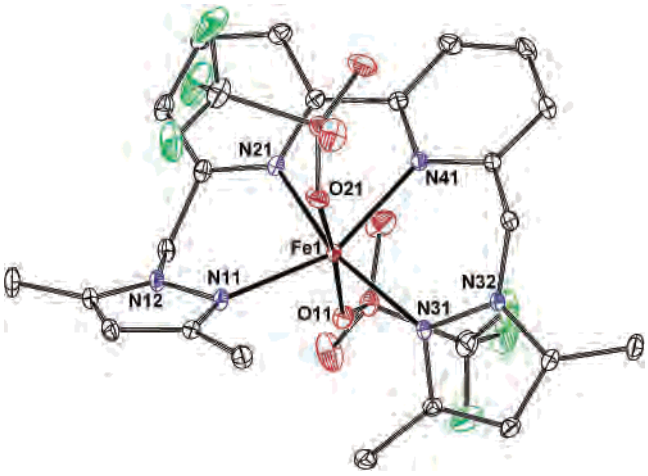

Figure 3. ORTEP view of [Fe(mbpzbpy)(CF_3SO_3)$_2$] (**2**) at the 30% probability level. Hydrogen atoms are omitted for clarity.

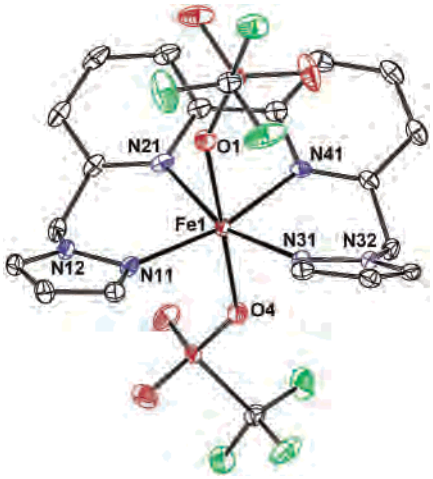

Figure 4. ORTEP view of [Fe(bpzbpy)(CF_3SO_3)$_2$] (**3**) at the 30% probability level. Hydrogen atoms are omitted for clarity.

molecules at normal distances of about 2.2 Å.[34] The equatorial N−Fe−N angles, varying from 75.88(8) to 107.07(8)°, reflect the strong geometric distortion induced by the bipyridine unit but also by the steric hindrance between two methyl groups of the pyrazole ligands. Accordingly, these steric interactions give rise to two enantiomeric forms, Δ and Λ (Figure 2). Considering the O3−Fe−O1 axis, the coordination of the N_4 ligand around the iron ion can indeed proceed in a clockwise (Δ) or an anticlockwise (Λ) manner. The resulting coordination enantiomers can only interchange through the dissociation of the pyrazoles (in solution).

Crystal Structure of [Fe(mbpzbpy)(CF_3SO_3)$_2$] (2). Reaction of the ligand mbpzbpy with iron(II) triflate in methanol results in complex **2**, which suggests that $CF_3SO_3^-$ is a less weakly coordinating anion, as compared to BF_4^-. Complex **2** crystallizes in the $P\bar{1}$ triclinic space group. An ORTEP perspective view of **2** is shown in Figure 3. Selected bond lengths and angles are given in Table 3. Similar to **1**, the unit cell contains two molecules **2** ($Z = 2$) which are enantiomers. The distorted [FeN_4O_2] octahedron is constituted of four nitrogen atoms at the basal plane (pyridine−Fe distances, Fe−N21 = 2.199(2) Å and Fe−N41 = 2.192(2) Å; pyrazole−Fe distances, Fe−N11 = 2.176(2) Å and Fe−N31 = 2.181(2) Å) and axially coordinated triflate anions (Fe−O11 = 2.164(2) Å, Fe−O21 = 2.221(2) Å). The basal angles (74.99(8)−110.12(8)°, Table 3) are once again clearly indicative of a strong distortion of the O_h geometry for which the four ideal angle values are 90°. This deformation from a perfect octahedral geometry is not only due to the small bite angle of the bipyridine fragment of the ligand but as well to the methyl substituents on the pyrazoles, as confirmed below with the examination of the crystal structure of complex **3**.

Table 3. Selected Bond Lengths (Å) and Angles (deg) in [Fe(mbpzbpy)(CF_3SO_3)$_2$] (**2**) and [Fe(bpzbpy)(CF_3SO_3)$_2$] (**3**)

Bond Distance			
2		**3**	
Fe1−N11	2.176(2)	Fe1−N11	2.122(3)
Fe1−N31	2.181(2)	Fe1−N31	2.147(3)
Fe1−N41	2.192(2)	Fe1−N41	2.155(3)
Fe1−N21	2.199(2)	Fe1−N21	2.167(3)
Fe1−O11	2.164(2)	Fe1−O4	2.125(3)
Fe1−O21	2.221(2)	Fe1−O1	2.229(3)
Bond Angle			
2		**3**	
N11−Fe1−N21	81.48(7)	N11−Fe1−N21	89.36(12)
N21−Fe1−N41	74.99(8)	N21−Fe1−N41	77.34(12)
N41−Fe1−N31	89.91(7)	N41−Fe1−N31	87.67(12)
N31−Fe1−N11	110.12(8)	N31−Fe1−N11	104.49(12)
O11−Fe1−O21	173.68(6)	O4−Fe1−O1	177.76(11)

Crystal Structure of [Fe(bpzbpy)(CF_3SO_3)$_2$] (3). The use of the demethylated ligand bpzbpy with iron(II) triflate in methanol leads to complex **3**. Complex **3** crystallizes in the $P2_1/n$ monoclinic space group. An ORTEP perspective view of **3** is shown in Figure 4. Selected bond lengths and angles are given in Table 3. The unit cell contains two pairs ($Z = 4$) of Δ/Λ enantiomers. As for **1** and **2**, the iron(II) center is in a distorted octahedral coordination environment. However, the distortion is smaller, as evidenced by the Fe−N distances and the basal N−Fe−N angles (Table 3). Indeed, the Fe−N_{py} bond lengths (Fe−N21 = 2.167(3) Å and Fe−N41 = 2.155(3) Å) and the Fe−N_{pz} bond lengths (Fe−N11 = 2.122(3) and Fe−N31 = 2.147(3) Å) are shorter compared to those of **1** and **2**, revealing a better coordination of the bpzbpy ligand around the iron(II) ion, since the complex does not experience steric repulsion due to the methyl groups. As a result, the ligand is more planar in complex **3** (for instance, the angle between the two pyrazole planes is 14° for **3**, while these angles amount to 72° and 71° for **1** and **2**, respectively). Accordingly, the basal angles of the octahedron are comprised in a smaller range, i.e., 77.34(12)−104.49(12)°, closer to 90°, by comparison with the values observed for **1** and **2** (Tables 2 and 3).

The steric hindrance of the methyl groups will prove to be crucial to explain the distinct magnetic properties observed for complexes **4** and **5** (see Magnetic Susceptibility Data).

Crystal Structure of [Fe(mbpzbpy)($NCS)_2$]($CH_3OH)_{0.5}$ (4). As aforementioned, the N_4 ligands mbpzbpy and bpzbpy (Chart 1, R = CH_3 and R = H, respectively) have been

(34) Roux, C.; Zarembowitch, J.; Gallois, B.; Bolte, M. *New J. Chem.* **1992**, *16*, 671−677.

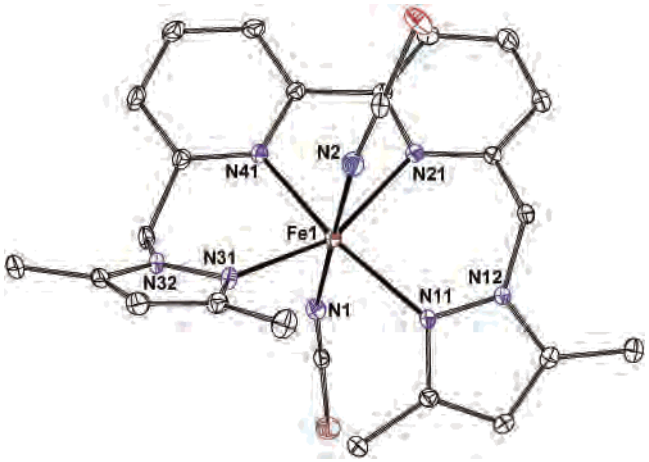

Figure 5. ORTEP view of $[Fe(mbpzbpy)(NCS)_2](CH_3OH)_{0.5}$ (**4**) at the 30% probability level. Methanol molecules and hydrogen atoms are omitted for clarity.

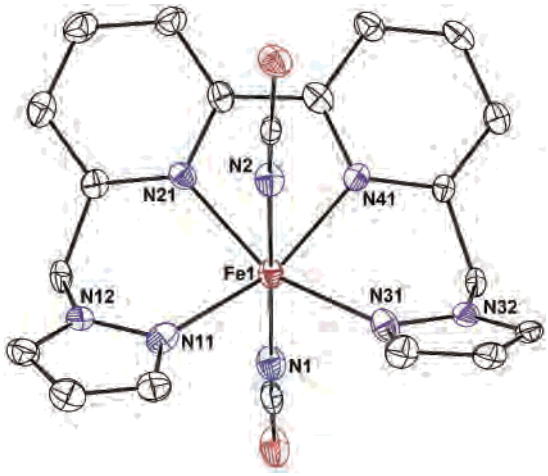

Figure 6. ORTEP view of $[Fe(bpzbpy)(NCS)_2]$ (**5**) at the 30% probability level. Hydrogen atoms are omitted for clarity.

designed to exclusively yield trans complexes (Figure S1) when coordinated to a metal ion, as achieved with compounds **1**−**3**. The objective is to produce octahedral iron(II) species bearing identical N_4 basal donor sets but with distinct monodentate axial ligands. For this purpose, complexes **2** and **3** are used as starting complexes since the weakly coordinated triflate anions allow the synthesis of axially modified iron(II) compounds through anion exchange. For instance, reaction of iron(II) triflate with the ligand mbpzbpy, followed by the addition of sodium(I) thiocyanate (see Experimental Section), produces complex **4**, where the $CF_3SO_3^-$ anions of **2** have been replaced by SCN^- anions (Figures 4 and 6). Complex **4** crystallizes in the $P\bar{1}$ triclinic space group. An ORTEP perspective view of **4** is shown in Figure 5. Selected bond lengths and angles are given in Table 4. The unit cell contains the two enantiomers of **4** ($Z = 2$). The coordination environment of the iron(II) ion in **4** is similar to the one observed in **2**. The $[FeN_6]$ octahedron is strongly distorted (Fe−N21 = 2.216(2) Å, Fe−N41 = 2.201(2) Å, Fe−N11 = 2.170(2) Å, and Fe−N31 = 2.201(2) Å) with basal angles varying from 74.42(7) to 109.08(7)°. The angle between the two pyrazole planes is 73°, in consequence of the steric interactions of two methyl groups of the coordinated pyrazoles. The axial positions are occupied by the nitrogen atoms of the thiocyanate anions at normal distances for HS Fe^{II} species (Fe−N1 = 2.151(2) Å and Fe−N2 = 2.193(2) Å).[35,36] In addition, **4** contains disordered methanol molecules in the crystal lattice.

Table 4. Selected Bond Lengths (Å) and Angles (deg) in $[Fe(mbpzbpy)(NCS)_2](CH_3OH)_{0.5}$ (**4**), and $[Fe(bpzbpy)(NCS)_2]$ (**5**)

Bond Distance			
4		**5**	
Fe1−N11	2.170(2)	Fe1−N11	2.124(4)
Fe1−N31	2.201(2)	Fe1−N31	2.128(3)
Fe1−N41	2.201(2)	Fe1−N41	2.205(4)
Fe1−N21	2.216(2)	Fe1−N21	2.191(4)
Fe1−N1	2.151(2)	Fe1−N1	2.115(5)
Fe1−N2	2.193(2)	Fe1−N2	2.208(4)
Bond Angle			
4		**5**	
N11−Fe1−N21	90.80(7)	N11−Fe1−N21	91.47(14)
N21−Fe1−N41	74.42(7)	N21−Fe1−N41	73.49(14)
N41−Fe1−N31	88.80(7)	N41−Fe1−N31	88.89(14)
N31−Fe1−N11	109.08(7)	N31−Fe1−N11	104.73(15)
N1−Fe1−N2	178.31(8)	N1−Fe1−N2	179.46(16)

Crystal Structure of $[Fe(bpzbpy)(NCS)_2]$ (5). Complex **5** has been prepared according to the procedure applied for the synthesis of **4** but using **3** as starting compound (see Experimental Section). Similarly to **3**, **5** crystallizes in the $P2_1/n$ monoclinic space group. An ORTEP perspective view of **5** is shown in Figure 6. The unit cell contains two pairs of enantiomers ($Z = 4$). Selected bond lengths and angles are given in Table 4. The $[FeN_6]$ octahedron is strongly distorted, with $Fe-N_{py}$ bonds (Fe−N21 = 2.191(4) Å and Fe−N41 = 2.205(4) Å) longer than the $Fe-N_{pz}$ ones (Fe−N11 = 2.124(4) Å and Fe−N31 = 2.128(3) Å). The basal N−C−N angles range from 73.49(14) to 104.73(15)°, which denote a slightly lesser distortion (comparison between **4** and **5**, Table 4) rising from inferior steric constraints (absence of methyl substituents on the pyrazole rings). As a result, the angle between the pyrazoles only amounts to 16° (the value for the corresponding methylated complex **4** is 73°). It has to be mentioned that these steric differences dramatically affect the magnetic properties of the resulting materials (see Magnetic Susceptibility Data).

Structure of $[Fe(bpzbpy)(NCSe)_2]$ (6). Because of the interesting physical properties of **5** (see Magnetic Susceptibility Data), its selenocyanate derivative,[37] namely, complex **6**, has been prepared from compound **3** in the presence of NaSeCN (see Experimental Section). This compound has only been obtained as a microcrystalline powder. Consequently, the single-crystal structure of **6** could not be determined. However, the elemental analyses as well as its magnetic properties (see below) suggest that complex **6** is comparable with **5**. Thus, its structure is expected to be the one shown in Figure 7, with $SeCN^-$ anions at the axial positions.

(35) Quesada, M.; Monrabal, M.; Aromi, G.; de la Pena-O'Shea, V. A.; Gich, M.; Molins, E.; Roubeau, O.; Teat, S. J.; MacLean, E. J.; Gamez, P.; Reedijk, J. *J. Mater. Chem.* **2006**, *16*, 2669−2676.
(36) Huang, W.; Ogawa, T. *J. Mol. Struct.* **2006**, *785*, 21−26.
(37) Sugiyarto, K. H.; Scudder, M. L.; Craig, D. C.; Goodwin, H. A. *Aust. J. Chem.* **2000**, *53*, 755−765.

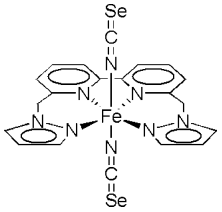

Figure 7. Schematic representation of [Fe(bpzbpy)(NCSe)$_2$] (**6**).

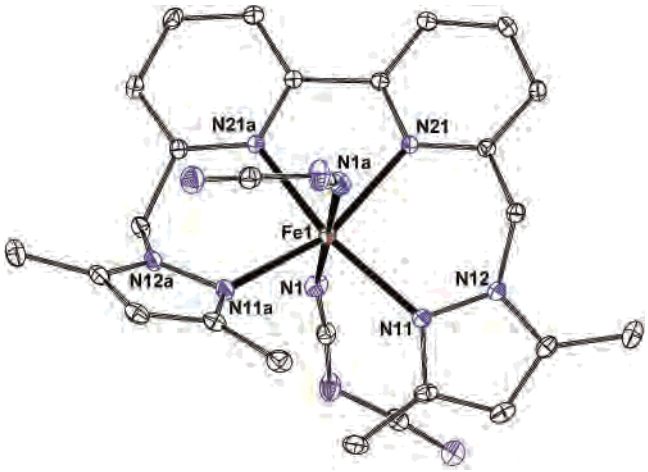

Figure 8. ORTEP view of [Fe(mbpzbpy)(N(CN)$_2$)$_2$] (**7**) at the 30% probability level. Hydrogen atoms are omitted for clarity.

Table 5. Selected Bond Lengths (Å) and Angles (deg) in [Fe(mbpzbpy)(N(CN)$_2$)$_2$] (**7**)

	Bond Distance		
Fe1−N11	2.175(2)	Fe1−N1	2.194(2)
Fe1−N21	2.200(2)		
	Bond Angle		
N11−Fe1−N21	90.51(6)	N21−Fe1−N21a	75.03(8)
N21a−Fe1−N11a	90.51(6)	N11a−Fe1−N11	107.28(9)
N1−Fe1−N1a	178.52(9)		

Crystal Structure of [Fe(mbpzbpy)(N(CN)$_2$)$_2$] (7). Complex **7** was prepared from **2** via the in situ addition of NaN(CN)$_2$ (see Experimental Section). Complex **7** crystallizes in the *C*2/*c* monoclinic space group. An ORTEP perspective view of **7** is shown in Figure 8. The unit cell contains two pairs of the two enantiomeric forms of **7** ($Z = 4$). Selected bond lengths and angles are given in Table 5. The [FeN$_6$] octahedron is strongly distorted, with longer Fe−N distances involving the bipyridine unit (Fe−N21 = Fe−N21a = 2.200(2) Å), compared to those with the pyrazoles (Fe−N11 = Fe−N11a = 2.175(2) Å). The equatorial N−Fe−N angles, varying from 75.03(8) to 107.28(9)°, reflect the geometric distortion generated by the small bite angle of the bipyridine unit. Once again, the steric interactions between the methylated pyrazoles lead to an angle of 78° between the corresponding planes. As for the previous coordination compounds, the crystal packing of **7** does not reveal any significant intermolecular interactions.

This last example involving an elongated anion, i.e., dicyanamide, further demonstrates the versatility of the synthetic procedure, which opens up the possibility to prepare extended structures (coordination polymers) via the axial coordination of multitopic ligands, pyrazine, 4,4′-bipyridine, 2,4,6-tris(4-pyridyl)-1,3,5-triazine, etc.

Magnetic Susceptibility Data. The temperature dependence of the $\chi_m T$ product of complexes **1**−**7** are reported in Table 6, where χ_m stands for the molar paramagnetic susceptibility and T the temperature. The magnetic susceptibility data were measured in the range 6−300 K, in both the cooling and the heating modes. From the magnetic data shown in Table 6, it appears that all complexes with the formula [Fe(mbpzbpy)L$_2$] (L = anion or solvent molecule; complexes **1**, **2**, **4**, and **7**) are high-spin state compounds throughout the whole temperature range. The room temperature $\chi_m T$ values ranging from 3.38 to 2.95 cm^3 mol^{-1} K characterize a $^5T_2$ ground-state ($S = 2$) in an octahedral coordination environment.[38] The same behavior is observed with [Fe(bpzbpy)(CF$_3$SO$_3$)$_2$] (**3**) with a $\chi_m T$ value of 3.03 cm^3 mol^{-1} K at room temperature. The plots of $\chi_m T$ vs T for complexes **5** and **6** are shown in Figures 10 and 11, respectively. Complexes [Fe(bpzbpy)(NCS)$_2$] (**5**) and [Fe(bpzbpy)(NCSe)$_2$] (**6**) exhibit a reversible change of color from purple (HS) to black (LS), indicative of spin-crossover behavior. The magnetic properties of **5** are depicted in Figure 9. The room temperature $\chi_m T$ value of 3.1 cm^3 mol^{-1} K corresponds to a high-spin state Fe^{II} species, with g close to 2. When cooled, this value remains constant until 200 K, where it starts to gradually decrease to reach a plateau at 1.20 cm^3 mol^{-1} K below 72 K. This plateau is observed within the temperature range 72−15 K and reveals an incomplete spin-transition. The subsequent drop of $\chi_m T$ at lower temperatures (below 15 K) can be attributed to the zero-field splitting of remaining HS Fe^{II} species. This type of gradual spin transition is commonly observed with iron(II) complexes based on multidentate ligands and suggests that the HS → LS transition is mostly governed by the first coordination sphere of the SCO center.[39] As aforementioned, this behavior can be explained by the absence of cooperativity between the iron(II) centers in **5**, as revealed by its crystal packing. The magnetic properties of [Fe(bpzbpy)(NCSe)$_2$] (**6**) are displayed in Figure 10. The $\chi_m T$ value at room temperature of 2.95 cm^3 mol^{-1} K corresponds to a high-spin iron(II) species ($S = 2$). When cooled, the $\chi_m T$ value decreases very gradually (during more than 200 K) to finally reach a $\chi_m T$ value of 0.60 cm^3 mol^{-1} K at very low temperatures, which is larger than the expected spin-only value for the d^6 LS state ($S = 0$). This behavior indicates that, similar to **5**, compound **6** undergoes an incomplete thermal spin-crossover.

Correlations between Magnetic and Structural Properties. The examination of the solid-state structures of **1**−**7** and their corresponding magnetic behaviors reveals some remarkable structure/property relationships. It is well established that the observation of the spin-crossover (SCO) phenomenon in iron(II) systems is associated with the crystal field on the metal center.[40] Thus, most of the SCO Fe^{II}

(38) Létard, J. F.; Guionneau, P.; Rabardel, L.; Howard, J. A. K.; Goeta, A. E.; Chasseau, D.; Kahn, O. *Inorg. Chem.* **1998**, *37*, 4432−4441.
(39) Toftlund, H.; McGarvey, J. J. *Top. Curr. Chem.* **2004**, *233*, 151−166.
(40) Lemercier, G.; Brefuel, N.; Shova, S.; Wolny, J. A.; Dahan, F.; Verelst, M.; Paulsen, H.; Trautwein, A. X.; Tuchagues, J. P. *Chem.—Eur. J.* **2006**, *12*, 7421−7432.

Table 6. Summary of the Magnetic Properties of Compounds **1**−**7**

compound[a]	T (K)	$\chi_m T$ ($cm^3\ mol^{-1}\ K$)	ground state
$[Fe(mbpzbpy)(MeOH)_2](BF_4)_2$ (**1**)	290−50	2.98	$^5T_2$
$[Fe(mbpzbpy)(CF_3SO_3)_2]$ (**2**)	290−50	3.02−3.01	$^5T_2$
$[Fe(bpzbpy)(CF_3SO_3)_2]$ (**3**)	290−50	3.03	$^5T_2$
$[Fe(mbpzbpy)(NCS)_2](CH_3OH)_{0.5}$ (**4**)	290−50	3.05−2.95	$^5T_2$
$[Fe(bpzbpy)(NCS)_2]$ (**5**)	290−50	3.12−1.18	$^5T_2 \leftrightarrow {}^1A_1$
$[Fe(bpzbpy)(NCSe)_2]$ (**6**)	290−50	2.95−0.62	$^5T_2 \leftrightarrow {}^1A_1$
$[Fe(mbpzbpy)(N(CN)_2)_2]$ (**7**)	290−50	3.38−3.40	$^5T_2$

[a] All coordination compounds exhibit a distorted octahedral geometry.

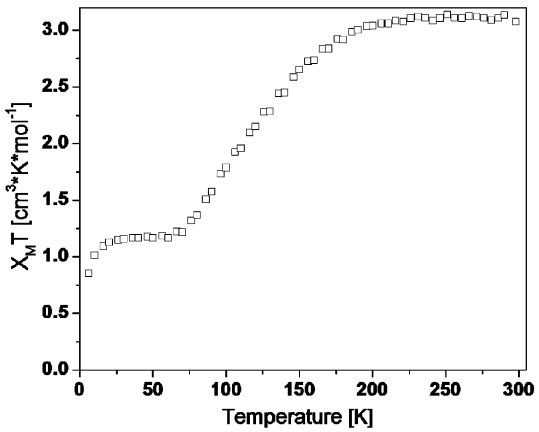

Figure 9. Plot of $\chi_m T$ vs T per molecule of a polycrystalline sample of $[Fe(bpzbpy)(NCS)_2]$ (**5**). The sample was cooled from 300 to 6 K at a rate of 3 K min^{-1}.

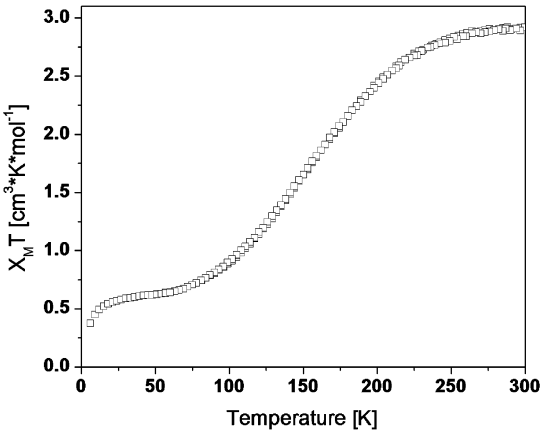

Figure 10. Plot of $\chi_m T$ vs T per molecule of a polycrystalline sample of $[Fe(bpzbpy)(NCSe)_2]$ (**6**). The sample was cooled from 300 to 6 K at a rate of 3 K min^{-1}.

compounds reported include a FeN_6 coordination sphere, where N almost exclusively represents an aromatic N-ligand.[11,41,42] In addition, coordinated thiocyanate and selenocyanate anions are known to favor the occurrence of the SCO phenomenon in octahedral iron(II) compounds.[40] These two features are clearly verified in the present study. Indeed, complex **3** exhibits a FeN_4O_2 core formed by one bpzbpy ligand and two axial triflate anions. This complex does not show a thermal HS−LS transition as a result of inappropriate ligand-field strength.[43] However, the in situ replacement of the triflates by thiocyanate anions (see Experimental Section) produces a SCO material, namely, complex **5**, which now presents a FeN_6 coordination sphere, obviously propitious to obtain the observed magnetic behavior. As expected, the exchange of the triflate anions by selenocyanate ones gives rise to the SCO complex **6**, since it is known that the ligand-field strength of the $SeCN^-$ ion is comparable to the one of the SCN^- anionic ligand.[44] These results show both that the magnetic properties of the complex can be fine-tuned through the judicious choice of the axial ligands and that these axial positions of the cationic species $[Fe^{II}(bpzbpy)]^{2+}$ can be easily exchanged without alteration of the metallic core. The latter observation opens the possibility to prepare $[Fe^{II}(bpzbpy)]^{2+}$-based extended structures, such as 1D polymeric chains, since ditopic ligands, i.e., bistetrazoles, bipyridines, and so on, may be used to replace the axial triflate ligands of **3**.

Another interesting feature is observed with complexes **4** and **5**. Indeed, these two structurally related FeN_6 compounds only differ by the presence or absence of methyl groups on the pyrazole rings (for **4** and **5**, respectively). However, their magnetic behaviors drastically diverge since **4** is purely a high-spin system, while **5** exhibits spin-crossover properties (Table 6). Such an effect of steric hindrance has already been observed with some ligand systems and used to fine-tune the crystal field.[39] For instance, the introduction of a steric bulk in the complex $[Fe(tptacn)](ClO_4)_2$[45] using the monomethylated ligand ^{Me}tptacn (^{Me}tptacn = *N*,*N*′-bis(2-pyridylmethyl),*N*′′-(6-methyl-2-pyridylmethyl)-1,4,7-triazacyclodecane) has allowed the conversion of the initial low-spin system into a spin-crossover compound.[39] Similarly, the use of 2-methyl phenanthroline (^{Me}phen) instead of phenanthroline (phen) within the low-spin cation $[Fe^{II}(phen)_3]^{2+}$ results in a spin-crossover $[Fe^{II}(^{Me}phen)_3]^{2+}$ system.[46] In the present study, the addition of steric bulk on the ligand converts the spin-crossover material **5** into the high-spin system **4** (see Table 6). Interestingly, the obvious steric interactions (Figure S2) induced by the incorporation of methyl substituents on the bpzbpy ligands do not seem to strongly weaken the ligand strength of the resulting mbpzbpy ligand. Indeed, The Fe−N_{ligand} bond distances at 173 K range from 2.170 to 2.216 Å and from 2.124 to 2.205 Å for **4** and **5**, respectively. Furthermore, the distortion of the octahedral geometry does not appear to be increased by steric effects due to the methyl

(41) Haasnoot, J. G. *Coord. Chem. Rev.* **2000**, *200*, 131−185.
(42) van Koningsbruggen, P. J. *Top. Curr. Chem.* **2004**, *233*, 123−149.
(43) Wilson, L. J.; Georges, D.; Hoselton, M. A. *Inorg. Chem.* **1975**, *14*, 2968−2975.
(44) *Chemie der Pseudohalogenide*; Golub, A. M., Köhler, H., Skopenko, V. V., Eds.; Elsevier: New York, 1986.
(45) Alobaidi, A. H. R.; McGarvey, J. J.; Taylor, K. P.; Bell, S. E. J.; Jensen, K. B.; Toftlund, H. *J. Chem. Soc., Chem. Commun.* **1993**, 536−538.
(46) Goodwin, H. A.; Kucharski, E. S.; White, A. H. *Aust. J. Chem.* **1983**, *36*, 1115−1124.

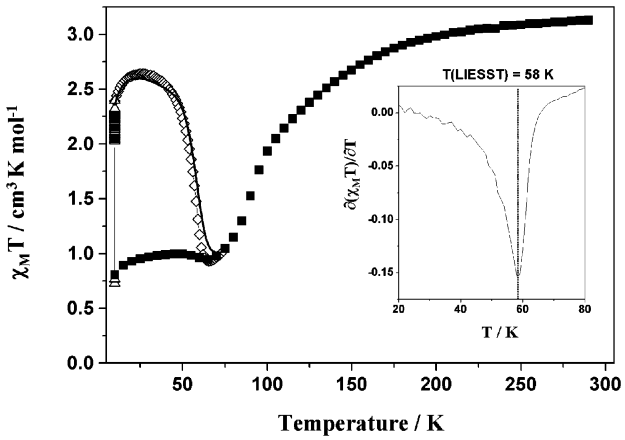

Figure 11. $\chi_m T$ vs T plot per molecule of a polycrystalline sample of [Fe(bpzbpy)(NCS)$_2$] (**5**). The temperature dependence of $\chi_m T$ recorded in the cooling mode without irradiation is symbolized by the ■ data. The sample was cooled from 300 to 6 K at a rate of 3 K min^{-1}. The change recorded during 1 h of irradiation at 10 K corresponds to the △ data, and the behavior recorded during the warming mode (0.3 K min^{-1}) after switching off the light irradiation is represented by the ◊ data. The insert graph shows the derivative d($\chi_m T$)/dT plot as a function of the temperature. The solid lines indicate the simulation obtained using the experimental kinetic parameters (E_a, k_∞, and Γ).

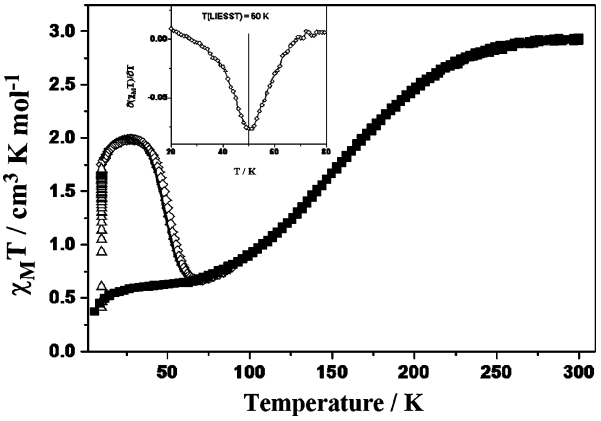

Figure 12. $\chi_m T$ vs T plot per molecule of a polycrystalline sample of [Fe(bpzbpy)(NCSe)$_2$] (**6**). The temperature dependence of $\chi_m T$ recorded in the cooling mode without irradiation is symbolized by the ■ data. The sample was cooled from 300 to 6 K at a rate of 3 K min^{-1}. The change recorded during 1 h of irradiation at 10 K corresponds to the △ data, and the behavior recorded during the warming mode (0.3 K min^{-1}) after switching off the light irradiation is represented by the ◊ data. The insert graph shows the derivative d($\chi_m T$)/dT plot as a function of the temperature. The solid lines indicate the simulation obtained using the experimental kinetic parameters (E_a, k_∞, and Γ).

groups (see angles around the metal centers in **4** and **5**, Table 4). By comparison, for the LS phen system, the coordination bond lengths vary from 1.967 to 1.980 Å at room temperature (295 K),[47] while at the same temperature, the ^{Me}phen values vary from 2.143 to 2.295 Å,[46] which are characteristic of HS species. In fact, contrary to the previously reported examples,[46,47] it appears that the methyl groups prohibit the corresponding system **4** to exhibit spin-transition properties. Two explanations may be found to clarify this behavior: (i) The methyl groups A and B (Figure S2b) do not allow the contraction of the octahedron typically observed during the HS → LS transition. Indeed, the two spin states differ on average in their coordination bonds by 0.2 Å,[48] and the strong steric interactions between the methyl substituents apparently prevent such shortening of the Fe−N distances. (ii) As clearly evidenced in Figure 12, the presence of the methyl groups in complex **4** significantly affects the coordination of the thiocyanate anions. While the thiocyanates are linearly coordinated to the iron(II) centers in **5** (Fe−N_{NCS}−C_{NCS} angles of 167 and 178°), a notable bend of these ions is clearly seen in compound **4** (Fe−N_{NCS}−C_{NCS} angles of 143 and 163°). As a result, the ligand-field strength of the thiocyanates is most likely reduced, which gives rise to a high-spin ground state. Furthermore, the close approach of the N_{NCS} donors to the iron(II) atom, required during the HS → LS transition, is hindered by the methyls, as mentioned above for the rigid tetradentate ligand.

Mössbauer Spectroscopy. ^{57}Fe Mössbauer spectra have been recorded at various temperatures in the range 4−300 K on crystalline samples of [Fe(bpzbpy)(NCS)$_2$] (**5**) (see Figure S3) and [Fe(bpzbpy)(NCSe)$_2$] (**6**). Selected spectral parameters are given in Tables S1 and S2 for complexes **5** and **6**, respectively (see Supporting Information).

At room temperature, **5** exhibits a doublet signal with a large quadrupole splitting (ΔE_Q = 2.61 mm s^{-1}) centered at an isomeric shift δ of 1.02 mm s^{-1}, characteristic of a HS iron(II) species (Table S1 and Figure S3). When the temperature is decreased, the quadrupole splitting of the HS species increases, which is a typical feature observed for iron(II) HS species, where the electric field gradient is dominated by the temperature-dependent valence-electron contribution.[11] The intensity of the HS signal decreases on lowering the temperature, while a new signal intensifies. This doublet signal with a small ΔE_Q (approximately 0.38 mm s^{-1}) centered at an isomeric shift δ of 0.507 mm s^{-1} is ascribed to iron(II) ions in the low-spin state (Table S1). The variation of the relative fraction of both doublets with temperature confirms the presence of a spin-crossover in **5**. As also evidenced by the magnetic susceptibility measurements (see above and Figure 9), the spin transition is incomplete, and the value of the residual HS fraction below 75 K is approximately 40% (Figure S3).

A comparable behavior is noticed with the ^{57}Fe Mössbauer features corresponding to complex [Fe(bpzbpy)(NCSe)$_2$] (**6**) (Table S2). The room temperature doublet signal with a large quadrupole splitting (ΔE_Q = 2.32 mm s^{-1}), attributed to the HS species, is centered at an isomeric shift δ of 1.03 mm s^{-1}. Upon the spin transition, the HS species are converted to LS species, which are characterized by ΔE_Q = 0.36 mm/s, δ = 0.49 mm/s. A remaining HS fraction of approximately 20% is observed below 50 K (Table S2), in agreement with the magnetic susceptibility study (see above and Figure 10).

Photomagnetism. The occurrence of a light-induced phenomenon at low temperature for compounds **5** and **6** was first investigated by diffuse absorption spectroscopy. When the compounds were cooled from room temperature down

(47) Baker, J.; Engelhardt, L. M.; Figgis, B. N.; White, A. H. *J. Chem. Soc., Dalton Trans.* **1975**, 530−534.
(48) Tuchagues, J. P.; Bousseksou, A.; Molnar, G.; McGarvey, J. J.; Varret, F. *Top. Curr. Chem.* **2004**, *235*, 85−103.

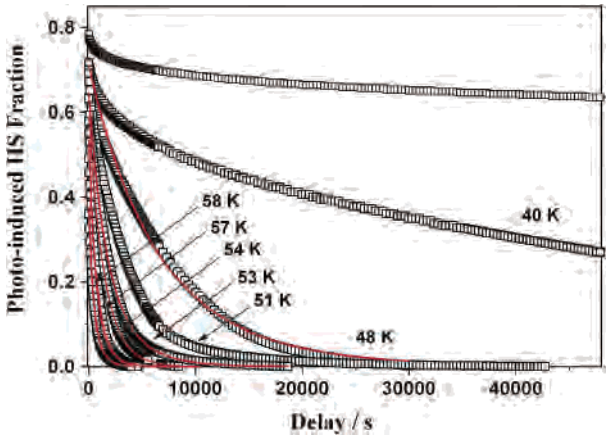

Figure 13. Time dependence at various temperatures of the HS molar fraction generated by laser irradiation of [Fe(bpzbpy)(SCN)$_2$] (**5**) at 10 K. Each point represents the high-spin fraction deduced from the magnetic response measured with the SQUID magnetometer during 30 s. The relaxation curves are fitted (solid lines) according to a stretched exponential behavior.

to the thermal spin transition, the absorption band centered at 850 nm, which is characteristic of d−d transitions for HS state species, decreases while absorption bands (MLCT and d−d transitions) in the visible range, ascribed to the LS state, increase (Figure S4a). An alternative manner to follow the changes in the diffuse absorption with the temperature is depicted in Figure S4c. This approach consists of determining the changes of the reflectivity spectra at a given selected wavelength, i.e., 560 nm. Along the thermal HS → LS spin transition, the absorption band at 560 nm increases, and consequently, the reflectivity signal decreases. Interestingly, below 75 K, the reflectivity signal of **5** (Figure S4c) starts to recover the magnitude of the signal at room temperature. This feature is also illustrated by the diffuse absorption spectrum recorded at 10 K as the shape of the 200 K spectrum (HS state) is recovered (Figure S4b). A comparable behavior is observed for complex **6**.

Both complexes thus exhibit surface light-induced phenomena, which indicate that the lifetime of the metastable photoinduced HS state below 50 K is sufficiently long to allow the optical excitation with a halogen light source. Additionally, the absence of a light-induced thermal hysteresis (LITH) loop[49] at low temperature, upon cooling and heating the sample under constant irradiation, is indicative of a weak cooperative photoinduced HS state.

The light-induced excited spin state trapping (LIESST) properties on bulk samples of **5** and **6** were investigated using a SQUID magnetometer. The sample was irradiated at 10 K at wavelength 532 nm, giving rise to an increase of the magnetic signal. After 1 h of irradiation, the $\chi_m T$ values were 2.35 cm^3 mol^{-1} K (**5**) and 1.75 cm^3 mol^{-1} K (**6**). The light source was then switched off, and the temperature was gradually increased at a rate of 0.3 K min^{-1} (Figures 11 and 12). Such procedure is typical to determine the limiting temperature T(LIESST) above which the light-induced magnetic high-spin information is erased in a SQUID cavity.[28,38] The increase of the magnetic signal with increasing temperature recorded below 30 K is consistent with the zero-field splitting expected for a HS iron(II) metal center in a nonperfect octahedral surrounding.[28,50] The maxima of the T(LIESST) curves are reached around 30 K for both compounds, corresponding to $\chi_m T$ values of 2.64 and 2.00 cm^3 mol^{-1} K for **5** and **6**, respectively. The differences observed in the $\chi_m T$ vs T plots depicted in Figures 9 and 11 for compound **5** most likely arise from a kinetic effect during the measurement due to different cooling rates as the measurements have been performed with two different SQUID magnetometers. On the basis of the magnetic values recorded at room temperature, it appears that 85% (**5**) and 70% (**6**) of the iron(II) centers involved in the SCO are converted to the HS states after irradiation. The minimum values of the d$\chi_m T$/dT vs T plots, which characterizes the T(LIESST) temperatures, amount to 58 K (**5**) and 50 K (**6**).

As depicted in Figure 13 for compound **5**, the relaxation curves at different temperatures can be satisfactorily fitted using a stretched exponential behavior, which is a typical feature for noncooperative SCO materials.[51,52] The apparent activation energies, $E_a = 490$ cm^{-1} (**5**) and $E_a = 250$ cm^{-1} (**6**), as well as the apparent pre-exponential factors of the activated region, $k_\infty = 3 \times 10^2$ s^{-1} (**5**) and $k_\infty = 2$ s^{-1} (**6**), are calculated from the plot ln $k_{HL}(T)$ vs $1/T$.[51] The distribution widths (Γ) of the activation energy using a Gaussian model are 15 and 50 cm^{-1} for **5** and **6**, respectively. Recently, it has been demonstrated that the determination of the kinetic parameters allows the T(LIESST) curve to be reproduced.[28,50] This procedure combines, in fact, both the temperature and the time dependencies, as well as the influence of the tunneling and the thermally activated regions. For noncooperative spin-crossover systems displaying a stretched exponential behavior, the T(LIESST) curve can be calculated by using a Gaussian distribution of individual T(LIESST) curves defined by each activation energy.[28] As evidenced in Figures 11 and 12, the calculated T(LIESST) curves are in good agreement with the experimental ones, indicating that both the experimental kinetics parameters used in this simulation and the fitting procedure are correct.

Conclusions

The rational design and synthesis of linear, rigid, (pyridine/pyrazole)-containing ligands have allowed the preparation of expected octahedral iron(II) coordination compounds, where the basal plane of the octahedron is fully occupied by the embracing N_4 ligands. This particular coordination geometry authorizes the exchange of the axial ligands without

(49) (a) Desaix, A.; Roubeau, O.; Jeftic, J.; Haasnoot, J. G.; Boukheddaden, K.; Codjovi, E.; Linares, J.; Nogues, M.; Varret, F. *Eur. Phys. J.* **1998**, *6*, 183−193. (b) Roubeau, O.; de Vos, M.; Stassen, A. F.; Burriel, R.; Haasnoot, J. G.; Reedijk, J. *J. Phys. Chem. Solids* **2003**, *64*, 1003−1013. (c) Létard, J. F.; Guionneau, P.; Rabardel, L.; Howard, J. A. K.; Goeta, A. E.; Chasseau, D.; Kahn, O. *Inorg. Chem.* **1998**, *37*, 4432−4441.

(50) Létard, J. F.; Chastanet, G.; Nguyen, O.; Marcen, S.; Marchivie, M.; Guionneau, P.; Chasseau, D.; Gütlich, P. *Monatsh. Chem.* **2003**, *134*, 165−182.

(51) Hauser, A.; Adler, J.; Gütlich, P. *Chem. Phys. Lett.* **1988**, *152*, 468−472.

(52) Létard, J. F.; Nguyen, O.; Soyer, H.; Mingotaud, C.; Delhaes, P.; Kahn, O. *Inorg. Chem.* **1999**, *38*, 3020−3021.

altering the overall coordination sphere around the iron(II) centers. Accordingly, a series of isostructural complexes have been obtained, whose magnetic properties solely depend on the nature, i.e., the ligand-field strength, of the axial ligands (anions or solvent molecules): due to the rigidity of the ligand, the physical properties (like the occurrence of the spin-transition phenomenon) are mostly governed by the first coordination sphere of the metallic centers, with hardly any cooperative interactions between them. In that manner, two uncommon SCO trans-compounds, i.e., **5** and **6**, could be prepared through the judicious choice of the axial ligands, thiocyanate and selenocyanate, respectively. These two SCO systems can be stimulated by means of both temperature variation and light irradiation. Drastic steric effects have been observed when methyl substituents are introduced in the ligand. Indeed, the SCO behavior is then lost, and it appears that the steric bulk (i) prevents the contraction of the octahedron (shortening of the Fe−N bond lengths) upon the HS → LS transition and (ii) induces a bending of the axial ligands with a subsequent modification of their ligand-field strength, which affects the electronic environment of the iron(II) centers.

This remarkable *trans*-FeN_4L_2 complex (L = axial ligand) is currently used to prepare potential cooperative SCO materials via the exchange of the monodentate axial L ligands with multitopic ones, which would favor the formation of 1D, 2D, or even 3D extended architectures and allow communication between metal ions.

Acknowledgment. This work has been supported financially by the Graduate Research School Combination "Catalysis", a joint activity of the graduate research schools NIOK, HRSMC, and PTN. Financial support from COST Action Grant Number D35/0011, Dutch WFMO (Werkgroep Fundamenteel-Materialen Onderzoek), CW (Foundation for the Chemical Sciences), NWO, and the DFG/CNRS bilateral program (DFG Project Gu 95/59) is gratefully acknowledged. Coordination by the FP6 Network of Excellence "Magmanet" (Contract Number 515767) is also kindly acknowledged.

Supporting Information Available: Mössbauer spectra and extended spectral parameters, reflectance spectra for complex **5**, and crystallographic information files (CIF format) of all newly characterized coordination compounds reported in this study. This material is available free of charge via the Internet at http://pubs.acs.org.

IC0624017